

Depth dependent local structures in thin films unraveled by grazing incidence x-ray absorption spectroscopy

Narcizo M. Souza-Neto,^{1,2,*} Aline Y. Ramos,^{3,1} Hélio C. N. Tolentino,^{3,1} Alessandro Martins,⁴ and Antonio D. Santos²

¹Laboratório Nacional de Luz Síncrotron, CP 6192, 13083-970, Campinas, Brazil

²Departamento de Física dos Materiais e Mecânica, Instituto de Física, Universidade de São Paulo, São Paulo, Brazil

³Institut Néel, CNRS et Université Joseph Fourier, BP 166, F-38042 Grenoble Cedex 9, France

⁴Universidade Federal de Goiás, Campus Jataí, Jataí, Brazil

A method of using X-ray absorption spectroscopy (XAS) together with resolved grazing incidence geometry for depth profiling atomic, electronic, chemical or magnetic local structures in thin films is presented. The quantitative deconvolution of thickness-dependent spectral features is performed by fully considering both scattering and absorption formalisms. Surface oxidation and local structural depth profiles in nanometric FePt films are determined, exemplifying the application of the method.

I. INTRODUCTION

Magnetic thin films have attracted a lot of attention due to their extremely high-density magnetic recording applications [1]. In this regard, a clear understanding of the macroscopic magnetic properties requires a substantial knowledge of its dependence with layers thicknesses [2] and the complex microstructural effects frequently localized at the interface with the substrate or the surface of the films. Such effects can be studied using experimental techniques able to peer selectively in the depth of the films. In a previous letter [3] we presented qualitative results using x-ray absorption spectroscopy (XAS) with resolved grazing incidence (GI) to clarify the thickness-dependent magnetic properties in nanometric CoPt films. A depth dependent chemical order was revealed and the magnetic behavior was interpreted within this framework. In the present paper we provide a rigorous quantitative method for the deconvolution of the local atomic, chemical and magnetic structural depth profiles. This method is then illustrated by its application to oxidized FePt thin films [4]. The proposed approach makes GI-XAS a unique tool to address the depth dependence of the local structural parameters, suitable for nanometric structures where this dependence is a crucial issue. Moreover this method provides a new venue to rigorously determine depth dependent electronic structure profiles using XANES (x-ray absorption near edge structure), which turns out to be crucial in understanding striking artificial interface materials [5, 6].

Although the general phenomena of scattering and absorption of x-rays by the condensed matter are nowadays quite well understood [7], they still are normally explored from unconnected viewpoints. A few well established techniques surpass this general rule with interconnected scattering and absorption techniques, providing invaluable additional selectivity compared to each approach used separately. DAFS (diffraction anomalous fine structure) gives site selectivity and local structural information [8]. XAFS (x-ray absorption fine structure) extracted from reflectivity data gives local structural

information from surfaces and interfaces [9]. XSW (x-ray standing wave) locates impurities in bulk crystals and nanostructures using an interference field that provides spatial dependence to the x-ray spectroscopic yields from atoms within the field [10]. Similarly, grazing-incidence x-ray fluorescence (GIXRF) is a sensitive probe of chemical composition as a function of depth [11]. These techniques are based on similar approaches to the one presented here, however they are limited to near-perfect crystal structures, require well defined geometries and/or give a limited set of information.

II. GRAZING INCIDENCE X-RAY ABSORPTION SPECTROSCOPY

X-ray absorption spectra contain information about the ground state of the selected element in a material (local symmetry, oxidation and spin states, spin-orbit coupling in the $2p$ and $3d$ orbitals, crystal field, covalence and charge transfer). As a matter of fact, in the case of $3d$ transition metals essentially structural information is obtained from the K edges, while more magnetic and electronic information is usually deduced from $L_{2,3}$ edge. XAS is not a surface technique by itself, since the attenuation length of hard x-rays is of a few micrometers in any material. However, in the grazing incidence geometry near the critical angle for total reflexion, the x-ray beam is confined within a few nanometers from the surface. For this film studies, this confinement has the considerable advantage of minimizing the substrate contribution.

The grazing incidence x-ray absorption measurements were performed at the Brazilian Synchrotron Light Laboratory (LNLS - Laboratório Nacional de Luz Síncrotron). The setup includes 20 μm -vertical slits limiting the beam size on the sample mounted on a high precision goniometer. XANES spectra were collected in the fluorescence mode at the D04B-XAFS1 beamline [12] with a Si (111) channel-cut monochromator. The incident beam intensity was monitored using a first ion-chamber. The reflected beam and fluorescence emission were simultaneously collected using a second ion-chamber and a 15-elements Ge detector, respectively. The fluorescence emission and/or x-ray reflectivity curves were used to calibrate and select with an accuracy of $\approx 0.01^\circ$ the working grazing angle corresponding to a chosen penetration depth profile.

*Present address: Advanced Photon Source, Argonne National Laboratory, Argonne, Illinois 60439, USA

For an accurate energy calibration, the transmission through an Iron metal reference foil was monitored using a third ion-chamber.

The collected absorption spectra measured by the fluorescence yield is a mix of contributions coming from different depths. To get quantitative information we must deconvolve them into their absorption contributions from each depth (z) into the films at each photon energy (E) and grazing angle (θ). The electromagnetic radiation amplitude at each set of (E , θ , z) must be known to weightly sum the absorption contributions as function of energy and angle ($\mu_{exp}(E, \theta)$), as follows:

$$\mu_{exp}(E, \theta) = \frac{1}{\Gamma} \int_0^{\infty} I(E, z, \theta) \mu(E, z) dz \quad (1)$$

where $I(E, z, \theta)$ is the radiation intensity as function of E , z and θ ; $\mu(E, z)$ is the absorption spectrum contribution at the depth z and Γ is the normalizing factor $\int_0^{\infty} I(E, z, \theta) dz$. The main difficulty to determine each $\mu(E, z)$ by solving this equation is the initial calculation of $I(E, z, \theta)$, which depends on how the layers structure of the film dynamically refract and reflect the incident radiation, as a function of energy and depth. The formalism adopted to determine this intensity and the way to extract the depth dependence from GI-XAS spectra are described in the following section.

A. Refracted and reflected amplitudes as a function of the penetration depth, photon energy and incident angle

Several approaches [7, 11, 13, 14, 15, 16, 17, 18, 19, 20, 21] can be used to estimate the transmissivity of x-rays inside a material. Those based on the dynamical diffraction theory give the most accurate results near the critical angle of total external reflection. We deal here with conditions near the critical energy and angle for absorption and reflectivity resonances. Hence the method must include all dynamical reflections and refractions conditions to determine the internal electromagnetic wave amplitude in the samples. To fulfill these requirements we apply an approach analogous to the recursive Parrat's reflectivity method [21] to calculate the refracted and reflected amplitudes at every depth within a film formed by n layers, each one with different chemical contributions.

Following the definitions by Parrat [21], we consider an electromagnetic wave propagating into a material:

$$\vec{E} = \vec{E}_0 e^{i[\hat{n}(\vec{k}\cdot\vec{r}) - \omega t]} = \vec{E}_0 e^{i[(1-\delta)(\vec{k}\cdot\vec{r}) - \omega t]} e^{-\beta(\vec{k}\cdot\vec{r})} \quad (2)$$

where δ and β are the real and imaginary part of the complex refraction index [7, 14, 22] $\hat{n} = 1 - \delta - i\beta$.

The continuity at each interface between the media n and $n-1$ of a film with N layers gives the twin equation :

$$\begin{aligned} a_{n-1} E_{n-1} + a_{n-1}^{-1} E_{n-1}^R &= a_n^{-1} E_n + a_n E_n^R \\ (a_{n-1} E_{n-1} + a_{n-1}^{-1} E_{n-1}^R) f_{n-1} k_1 &= (a_n^{-1} E_n + a_n E_n^R) f_n k_1 \end{aligned} \quad (3)$$

where $f_n = (\theta_n^2 - 2\delta_n - 2i\beta_n)^{1/2}$ for each n media and $a_n = e^{-i\frac{\pi}{\lambda} f_n d_n}$ is a phase factor taking into account the absorption,

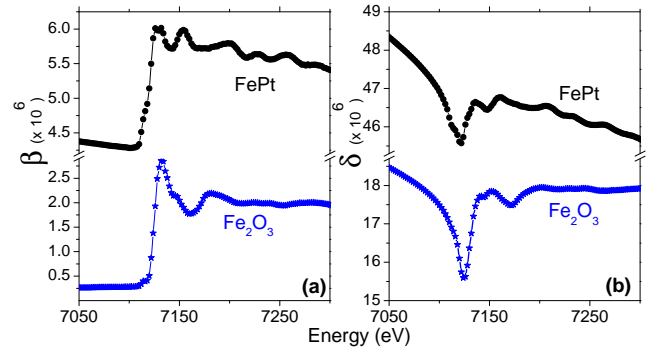


Figure 1: (color online) Experimental refraction index $\hat{n} = 1 - \delta - i\beta$ corresponding to FePt and Fe₂O₃. In (a) is the imaginary β component, and the real δ component obtained with Kramers-Kronig transform is in (b).

where d_n is the half penetration in the media n . E_n and E_n^R are the total and reflected electric field amplitudes in the media n . The solution of the equation 3 for the reflected amplitude $R_{n-1,n}$ can be recursively determined by

$$R_{n-1,n} = a_{n-1}^4 \left[\frac{F_{n-1,n} + R_{n,n+1}}{1 + R_{n,n+1} F_{n-1,n}} \right] \quad (4)$$

where $F_{n-1,n} = \frac{f_{n-1} - f_n}{f_{n-1} + f_n}$ and $R_{n,n+1} = a_n^2 (E_n^R / E_n)$.

The reflectivity at the interface between the air (or vacuum) and the film is obtained after previous determination of $R_{n-1,n}$ at all others interfaces inside the film, considering that $R_{N-1,N} = 0$, as the infinitely thick substrate does not add any reflection.

The electromagnetic radiation amplitude at each depth (z) inside a thin film can be determined in the same way by solving the equations 3 to inform the amplitude E_n at each layer n and depth z . Isolating E_n in equation 3 and using the value $R_{n-1,n} = a_{n-1}^2 (E_{n-1}^R / E_{n-1})$, one straightforwardly obtains:

$$E_n = a_n a_{n-1} \left(\frac{1 + \frac{F_{n-1,n} + R_{n,n+1}}{1 + R_{n,n+1} F_{n-1,n}}}{1 + R_{n,n+1}} \right) E_{n-1} \quad (5)$$

E_n can be recursively determined from the previous knowledge of the elements $R_{n,n+1}$ and $F_{n-1,n}$ calculated for the total reflectivity. Consequently, the amplitude at the upper interface of layer n is :

$$b_n = \frac{E_n}{a_n E_0} (1 + R_{n,n+1}) \quad (6)$$

with E_0 incident amplitude on the film surface ($n = 0$).

The amplitude inside the layer n at an arbitrary position z_n relative to the top of the layer is then $B_n = b_n \cdot e^{-i\frac{2\pi}{\lambda} f_n z_n}$ and the radiation intensity inside this layer n is $I_n(z_n, \theta, E) = |b_n \cdot e^{-i\frac{2\pi}{\lambda} f_n z_n}|^2$. The total intensity $I(z, \theta, E)$ at each depth z is given by the set of $I_n(z_n, \theta, E)$ considering each thicknesses d_n and all possible n . The angle and energy dependences contained in the $f_n(\delta, \beta, \theta)$ complex terms are fully mathematically and computationally considered, where β and δ are the

components of the refraction index, as shown in figure 1 for FePt and Fe₂O₃ compounds.

B. Depth dependence of XAS spectra

The electromagnetic radiation intensity $I(E, z, \theta)$ described above is used to determine the depth profile of XANES experimentally obtained in the grazing incidence geometry. This is performed by fitting XANES spectra for several grazing angles around the critical angle, considering the x-ray attenuation inside the material. The result of this process is the stratification in layers (of thickness dz) of the XANES information. The XANES spectra for each depth are fitted as a linear combination of reference spectral contributions previously determined. As the structure of layers inside the film can change dynamically in the fitting process, the $I(z, \theta, E)$ intensity must be calculated at each self-consistent fitting iteration.

To determine the depth dependence of μ_{exp} , it must be found a set of $\mu(E, z)$ data that when convoluted with $I(E, z, \theta)$ in the equation 1 simultaneously fits $\mu_{exp}(E, \theta)$ measured for several θ . This is more easily done rewriting the equation 1 in a discrete form considering the sum in z with steps of Δz in depth:

$$\mu_{exp}(E, \theta) = \frac{1}{\Gamma} \sum_{i=0}^{\infty} I(E, z_i, \theta) \mu(E, z_i) \quad (7)$$

where $z_0 = 0$, $z_{\infty} = \infty$, $z_{i+1} - z_i = \Delta z$ and $\Gamma = \sum_{i=0}^{\infty} I(E, z_i, \theta)$.

It is easily seen that the proportional contribution (PC) for each Δz layer at depth z_i for the signal $\mu_{exp}(E, \theta)$ is determined by $PC(z_i) = I(E, z_i, \theta)/\Gamma$. If the experimental spectra can be considered as a linear combination of several independent contributions of XANES features, $\mu_{exp}(E, \theta)$ can be considered as a linear combination of q spectral contributions (j) each one weighed by a factor w_j :

$$\mu_{exp}(E, \theta) = \frac{1}{\Pi} \sum_{j=1}^q \mu_j(E) \cdot w_j(\theta) \quad (8)$$

where Π is the normalization factor $\Pi = \sum_{j=1}^q w_j(\theta)$.

Considering the equations 7 and 8, each $\mu(E, z_i)$ can be written as $\mu(E, z_i) = \frac{1}{\Pi} \sum_{j=1}^q \mu_j(E) \cdot w_j(z_i)$ where $\Pi(z_i) = \sum_{j=1}^q w_j(z_i)$. Therefore:

$$\mu_{exp}(E, \theta) = \frac{1}{\Gamma} \sum_{i=0}^{\infty} \frac{1}{\Pi} \sum_{j=1}^q I_j(E, z_i, \theta) \cdot \mu_j(E) \cdot w_j(z_i) \quad (9)$$

The objective of determining all absorption contributions ($\mu_j(E)$) and its equivalent weight ($w_j(z_i)$) for each depth z_i can be achieved by fitting the experimental spectra $\mu_{exp}(E, \theta)$ with equation 9. Is important to note that since $\beta(E)$ for each spectral contribution at each layer is included on both $I(E, z, \theta)$ and $\mu(E, z)$ of equation 7, the deconvolution of $\mu_{exp}(E, \theta)$ must be a self-consistent procedure in terms of β . In other words, $I(E, z, \theta)$ must be computed at every iteration of the $\mu_{exp}(E, \theta)$ fitting procedure.

III. APPLICATION: DEPTH PROFILE IN A FEPT MAGNETIC THIN FILM

The FePt film studied here was grown by sputtering from pure targets of elemental Fe and Pt. It was deposited on MgO(100) substrate with a pre-deposited Pt fcc(100) buffer layer. The substrate temperature was kept at 500°C to ensure a good chemical order and perpendicular magnetic anisotropy [4]. The composition and thickness of the film was checked by Rutherford Backscattering Spectroscopy (RBS) confirming the equiatomic ratio (51% Fe and 49% Pt) and a thickness of 103 nm for the FePt layer.

When deposited at high substrate temperature (> 400°C) FePt thin films without cap layer protection are easily oxidized materials [23]. The presence of a surface oxidation is clearly observed in the GI-XAS measurements at the smallest grazing angle presented on figure 2, and the oxide is identified as Fe₂O₃. The contribution of the oxide layer decreases rapidly for increasing angles, indicating that this layer is limited to a few Å. This is clearly seen by the decreasing (increasing) feature at 7133 (7115) eV and the shift of the spectra to lower energies presented in figure 2 (upper inset).

Simple tabled or calculated δ and β components of the refraction index $\hat{n} = 1 - \delta - i\beta$ [14, 22] cannot be used to calculate $I(E, z, \theta)$, given that it would include approximations not valid when the spectral features near a critical energy (absorption edge) are the desired information. The imaginary β component of the experimental refraction index was obtained for reference FePt and Fe₂O₃ samples using their absorption spectra scaled to tabled absolute values far from the absorption edges [14, 22], as shown in figure 1a. Kramers-Kronig transforms [24, 25, 26, 27, 28, 29, 30] were used to determine the correspondent real δ component (fig. 1b). Figure 3 shows the simulated intensity $I(E, z, \theta)$ for a model thick FePt film with a flat 5 nm Fe₂O₃ layer on its surface, using equation 6 and the refraction index data for each layer presented in figure 1. The XANES structures must definitively be taken into account when determining the experimental refraction index in order to include all energy/angle dependences in $I(E, \theta)$, as is ratified by the strong non-linear dependence on $I(E)$ for different grazing angles shown in fig. 3a. The intensity $I(\theta)$ at $E = 7130$ eV for representative z values is shown in fig. 3b, which exemplifies multiple reflection interference effects near the critical angle for each penetration. The interference condition for the first Fe₂O₃ layer (5 nm) is drastically different from the resonances for the deeper layers, where the contributions arise essentially from the FePt alloy. These simulations emphasizes the strong need to consider all dynamical reflections at the interfaces to accurately calculate $I(E, z, \theta)$.

On the other hand it is worth noting that although corrections due to fluorescence self-absorption effects might be important in some cases, these effects are not significant for the angular range and penetration depth discussed here (<1% in the final error bars).

Equation 9, considering the iteratively determined $I(E, z, \theta)$, was used to simultaneously fit the experimental XANES spectra taken at several grazing angles (fig. 2). Reference XANES spectra of Fe₂O₃ and FePt were used in

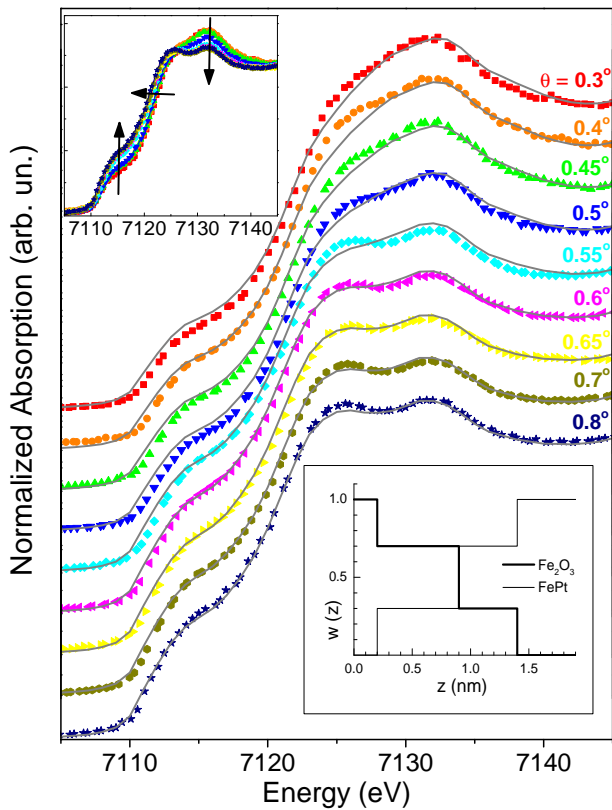


Figure 2: (color online) Fitted XANES experimental data as a function of the energy and several grazing angles for a FePt film. The best model to fit the experimental data consists of a gradient between a oxidated surface with pure Fe_2O_3 layer (0.2 nm thick), with intermediary layers of both oxide and metal (0.7 and 0.5 nm thick), to the pure FePt metal inside the films. Upper inset : GI-XAS measurements for increasing grazing angles showing the dependence of the XANES features as a function of the penetration depth, or grazing angle. The arrows correspond to an increase in the grazing angle. Lower inset: weight function w for the two components (Fe_2O_3 and FePt), for the oxidation profile corresponding to the best fit.

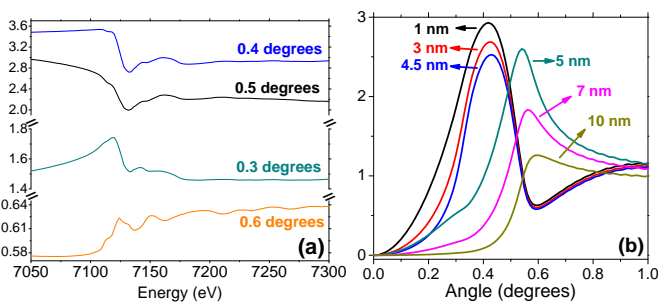


Figure 3: (color online) Calculated intensity of the electromagnetic radiation inside a thin film of $[\text{Fe}_2\text{O}_3]_{5\text{nm}}/[\text{FePt}]_{95\text{nm}}/[\text{Pt}]_{50\text{nm}}/\text{MgO}$. In (a) is the intensity as function of photon energy and grazing angle, at fixed penetration of 2 nm. In (b) is the dependence with incident angle and the depth penetration, with fixed energy of 7130 eV.

the fit.

The several experimental spectra simultaneously fitted, shown in figure 2, enable us to determine the complex layers structure in the depth profile, beyond a simply oxidized thickness determination. Different models of layers structure were considered for the oxidized FePt surface. Although a flat top oxide layer is well-suited to illustrate the general behavior, it is by far not the right solution to fit our data. The depth profile analysis shows clearly that the oxide not only covers the FePt film but penetrates beneath the film giving rise to a fractionated buried layer composed of the oxide and FePt. The best fit model turns out to be a gradient between a thin oxidized surface with pure Fe_2O_3 layer and intermediate layers of both oxide and metal alloy down to 1.4 nm from the surface. The top 100% oxide layer is 0.2 nm thick, followed by two mixed layers with 70% and 30% of Fe_2O_3 and 0.7 and 0.5 nm thick, respectively. The weight function w for each component is shown in the lower inset in figure 2.

It has been reported [23] that for FePt films an Fe oxide layer would form on the surface due to Fe migration to the oxide/metal interface during the growth at high temperatures. As a result, there might be a composition variation with increasing film depth. In the metallic layer just below the oxide, Fe content should be lower than that of as-deposited film while Pt content should be higher. Our results confirm a compositional variation over the film depth, but supports a more complex picture. As known from literature, sputtered metallic films have some tendency to form pillars. We interpret the gradient as resulting from the decoration of these pillars by the oxide that fills the empty space between pillars and oxidizes the very interfacial Fe atoms, rather than a continuous rough surface.

We should finally include an additional remark about the resolution of the depth profiles. Due to the exponential decay of the radiation intensity inside the film, the depth probed and final resolution of the method are intrinsically correlated and strongly dependent to the contrast between the refraction index of each layer material in the film. For instance, in the $\text{Fe}_2\text{O}_3/\text{FePt}$ case the refraction index of Fe_2O_3 is factor three smaller than for the FePt material. In this case the profile variation is confined within 2 nm near the surface and the depth resolution is of order of one angstrom. If the compositional gradient were deeper into the film, the profile resolution would be lower for the internal layers.

IV. CONCLUSION

Scattering and absorption phenomena are intrinsically intercorrelated when grazing incidence reflection and refraction are combined to x-ray absorption spectroscopy. The approach of GI-XAS presented in this article fully considers both scattering and absorption formalism for depth profiling the atomic, electronic, chemical or magnetic local structures in thin films with nanometric resolution. This formalism, not facing intrinsic limitations or approximations, can be applied to deconvolve the depth dependencies of not only XANES information as exemplified here, but also XRF (x-ray fluores-

cence) and XMCD (x-ray magnetic circular dichroism) signals in the fluorescence or reflectivity channels from thin films and multilayers.

Acknowledgments

This work is partially supported by LNLS/ABTLuS/MCT. NMSN acknowledges the grants from CNPq and CAPES.

-
- [1] D. Weller and M. F. Doerner, *Annual Review of Material Science* **30**, 611 (2000).
- [2] M. T. Johnson, P. J. H. Bloemen, F. J. A. den Broeder, and J. J. de Vries, *Rep. Prog. Phys* **59**, 1409 (1996).
- [3] N. M. Souza-Neto, A. Y. Ramos, H. C. N. Tolentino, A. Martins, and A. D. Santos, *Appl. Phys. Lett.* **89**, 111910 (2006).
- [4] A. Martins, M. C. A. Fantini, N. M. Souza-Neto, A. Y. Ramos, and A. D. Santos, *J. Magn. Magn. Mat.* **305**, 152 (2006).
- [5] N. M. Souza-Neto, D. Haskel, Y. C. Tseng, and G. Lapertot, *Phys. Rev. Lett.* (in press) [arxiv/0808.0865](https://arxiv.org/abs/0808.0865), 1 (2009).
- [6] J. Chakalian, et al., *Science* **318**, 1114 (2007).
- [7] J. Als-Nielsen and D. McMorrow, *Elements of Modern X-ray Physics* (John Wiley and Sons, 2001).
- [8] H. Stragier, et al., *Phys. Rev. Lett.* **69**, 3064 (1992).
- [9] P. Keil, D. Lutzenkirchen-Hecht, and R. Frahm, *Europhysics Letters* **71**, 77 (2005).
- [10] M. J. Bedzyk, G. M. Bommarito, and J. S. Schildkraut, *Phys. Rev. Lett.* **62**, 1376 (1989).
- [11] D. K. G. deBoer, *Phys. Rev. B* **44**, 498 (1991).
- [12] H. C. N. Tolentino, et al., *J. Synchrotron Rad.* **8**, 1040 (2001).
- [13] M. Born and E. Wolf, *Principles of Optics: Electromagnetic theory of propagation, interference and diffraction of light* (Pergamon Press, 1993).
- [14] B. L. Henke, E. M. Gullikson, and J. C. Davis, *Atomic Data and Nuclear Data Tables* **54**, 181 (1993).
- [15] W. B. Yun and J. M. Bloch, *J. Appl. Phys.* **68**, 1421 (1990).
- [16] P. Mikulík, Ph.D. thesis, Université Joseph Fourier - Grenoble I (1997).
- [17] A. Authier, *Dynamical Theory of X-Ray Diffraction* (Oxford University Press, 2001).
- [18] A. Q. R. Baron, Ph.D. thesis, Stanford University (1995).
- [19] S. A. Stepanov, et al., *Physical Review B* **57**, 4829 (1998).
- [20] D. R. Lee, et al., *Physical Review B* **68**, 224409 (2003).
- [21] L. G. Parrat, *Phys. Rev.* **95**, 359 (1954).
- [22] C. T. Chantler, *J. Phys. Chem. Ref. Data* **29**, 597 (2000).
- [23] K. Na, J. Na, H. Kim, P. Jang, and S. Lee, *IEEE TRANSACTIONS ON MAGNETICS* **37**, 1302 (2001).
- [24] K. Ohta and H. Ishida, *Applied Spectroscopy* **42**, 952 (1988).
- [25] J. E. Bertie and S. L. Zhang, *Can. J. Chem.* **70**, 520 (1992).
- [26] C. W. Peterson and B. W. Knight, *Journal Of The Optical Society Of America* **63**, 1238 (1973).
- [27] J. J. Hoyt, D. DeFontaine, and W. K. Warburton, *Journal Of Applied Crystallography* **17**, 344 (1984).
- [28] F. W. King, *J. Opt. Soc. Am. B* **19**, 2427 (2002).
- [29] F. W. King, *Journal Of Physics A-Mathematical And General* **39**, 10427 (2006).
- [30] J. O. Cross and A. I. Frenkel, *Rev. Sci. Instrum.* **70**, 38 (1999).